frontiers | Frontiers in Chemistry

ORIGINAL RESEARCH
published: 25 July 2022
doi: 10.3389/fchem.2022.934048

The First-Principles Study of External Strain Tuning the Electronic and Optical Properties of the 2D $MoTe_2$/PtS_2 van der Waals Heterostructure

Li Zhang[1], *Kai Ren*[2,3], *Haiyan Cheng*[4], *Zhen Cui*[5] *and Jianping Li*[6]*

[1]Department of Application & Engineering, Zhejiang Institute of Economics and Trade, Hangzhou, China, [2]School of Mechanical and Electronic Engineering, Nanjing Forestry University, Nanjing, China, [3]School of Mechanical Engineering, Wanjiang University of Technology, Maanshan, China, [4]School of Foreign Languages, Zhejiang University of Finance & Economics Dongfang College, Zhejiang, China, [5]School of Automation and Information Engineering, Xi'an University of Technology, Xi'an, China, [6]School of Automotive & Transportation Engineering, Shenzhen Polytechnic, Shenzhen, China

Two-dimensional van der Waals (vdW) heterostructures reveal novel properties due to their unique interface, which have attracted extensive focus. In this work, the first-principles methods are explored to investigate the electronic and the optical abilities of the heterostructure constructed by monolayered $MoTe_2$ and PtS_2. Then, the external biaxial strain is employed on the $MoTe_2$/PtS_2 heterostructure, which can persist in the intrinsic type-II band structure and decrease the bandgap. In particular, the $MoTe_2$/PtS_2 vdW heterostructure exhibits a suitable band edge energy for the redox reaction for water splitting at pH 0, while it is also desirable for that at pH 7 under decent compressive stress. More importantly, the $MoTe_2$/PtS_2 vdW heterostructure shows a classy solar-to-hydrogen efficiency, and the light absorption properties can further be enhanced by the strain. Our results showed an effective theoretical strategy to tune the electronic and optical performances of the 2D heterostructure, which can be used in energy conversion such as the automotive battery system.

Keywords: vdW heterostructures, first-principles method, $MoTe_2$/PtS_2, strain, solar-to-hydrogen efficiency

OPEN ACCESS

Edited by:
Guangzhao Wang,
Yangtze Normal University, China

Reviewed by:
San-Dong Guo,
Xi'an University of Posts and Telecommunications, China
Sake Wang,
Jinling Institute of Technology, China

***Correspondence:**
Jianping Li
szyljp0170@szpt.edu.cn

Specialty section:
This article was submitted to Theoretical and Computational Chemistry, a section of the journal Frontiers in Chemistry

Received: *02 May 2022*
Accepted: *24 May 2022*
Published: *25 July 2022*

Citation:
Zhang L, Ren K, Cheng H, Cui Z and Li J (2022) The First-Principles Study of External Strain Tuning the Electronic and Optical Properties of the 2D $MoTe_2$/PtS_2 van der Waals Heterostructure. Front. Chem. 10:934048. doi: 10.3389/fchem.2022.934048

INTRODUCTION

Graphene shows unique electronic and thermal performances after being prepared as a two-dimensional (2D) material (Geim and Novoselov, 2007), which has also attracted other layered materials (Cui et al., 2021a; Cui et al., 2021b; Ren et al., 2022a; Wang et al., 2022a). However, its zero bandgap restricts the applications as electronic switch and other devices. Therefore, 2D semiconducting materials include transition metal dichalcogenides (TMDs) (Shen et al., 2022), phosphorene, and MXenes. MoS_2 possesses excellent electronic and photoelectric properties similar to or even more advantageous than graphene in some aspects (Butler et al., 2013; Zhang et al., 2018). After the successful synthesis of graphene and MoS_2, more and more 2D materials have been found and synthesized. Its direct bandgap is about ~1.8 eV (Wickramaratne et al., 2014), which can be widely used in transistors, optoelectronics, and photocatalysts (Radisavljevic et al., 2011; Qiu et al., 2013; Ma et al., 2020). Black phosphorene has intrinsic direct bandgap and high carrier mobility (Li et al., 2014). Due to the anisotropic structure, black phosphorene shows remarkable anisotropic electronic, mechanical, and thermal properties. All these excellent properties endow its application in high-performance photovoltaic (Liu et al.,

2017), spin-filter devices (You et al., 2016), thermal rectifiers (Ren et al., 2020a), field-effect transistors (Hong et al., 2014), etc.

To expand the family of 2D materials, tremendous investigations have been conducted to predict the structure and properties of these layered materials (Sun et al., 2020; Sun and Schwingenschlögl, 2020; Sun et al., 2021; Sun and Schwingenschlögl, 2021). In addition, the formation of the van der Waals (vdW) heterostructure by different 2D materials is also a popular strategy to extend the applications of the 2D materials (Wang et al., 2022b). The vdW interactions in the heterostructure result in novel interfacial performances, which can improve the electronic (Ren et al., 2021a), optical (Ren et al., 2019a), and catalytic (Wang et al., 2018a; Wang et al., 2020a; Wang et al., 2020b) characteristics. Furthermore, such excellent properties of the heterostructure can even be tuned by the electric field (Sun et al., 2017a), strain (Ren et al., 2019b; Wang et al., 2020c; Wang et al., 2020d), stacking (Ren et al., 2022b), doping (Ren et al., 2022c),and defect (Sun et al., 2017b). When applied, the external strain is an effective tactic; for example, the band structure of the MXene/blue phosphorene vdW heterostructure can result in the transformation from type-I to type-II by the strain (Guo et al., 2017). The external strain also possesses a significant influence on the layer distance, which further decides the interfacial performances (Guo et al., 2020). Under the strain, the evolution of Schottky barriers of the GaN/graphene heterostructure can be converted from the n-Schottky to Ohmic type (Deng and Wang, 2019). Recently, the TMD materials of $MoTe_2$ and PtS_2 monolayers have been prepared experimentally (Qu et al., 2017; Zhao et al., 2019). The $MoTe_2$ and PtS_2 monolayers present the novel electronic (Qu et al., 2017; Sajjad et al., 2018) and thermoelectric (Shi et al., 2017) properties, which have been widely studied. The 2D $MoTe_2$ can be obtained from mechanically exfoliated bulk crystals (Chang et al., 2016), which have potential usages in electronics, such as inverters and amplifiers, and in logic and digital circuits. Moreover, the electronic property of $MoTe_2$ is sensitive to atomic doping (Kanoun, 2018), suggesting tunable electronic and optical performances. The PtS_2 monolayer also presents tunable properties by the strain (Liu et al., 2018) and electric field (Nguyen et al., 2019). In addition, the PtS_2 monolayer is reported to be formed as a vdW heterostructure such as PtS_2/arsenene (Ren et al., 2020b), PtS_2/InSe (Nguyen et al., 2019), and HfS_2/PtS_2 (Colibaba et al., 2019). Furthermore, the $MoTe_2$ and PtS_2 monolayers share a honeycomb hexagonal structure with a small lattice mismatch, explaining the advantage to be formed as a heterostructure. Therefore, the $MoTe_2$ and PtS_2 monolayers have been decided to be used for constructing the heterostructure in this work. The first-principles calculations are developed to investigate the band structure of the $MoTe_2/PtS_2$ (MP) heterostructure. Importantly, the tunable electronic, charge density, potential, light absorption ability, and the solar-to-hydrogen efficiency (STH) by the external biaxial strain are addressed.

COMPUTATIONAL METHODS

In this investigation, the Vienna *ab initio* simulation software package (VASP) was used to find the first-principles simulations by the density functional theory (DFT) (Kresse and Furthmüller, 1996a; Kresse and Furthmüller, 1996b). In the generalized gradient approximation (GGA), the projector augmented wave (PAW) potentials were used with the Perdew–Burke–Ernzerhof (PBE) functional to describe the core electrons and the exchange–correlation functional (Perdew et al., 1996; Kresse and Joubert, 1999). The cut-off energy was used by 550 eV, and the Monkhorst–Pack *k*-point was 15 × 15 × 1 in the calculations. Furthermore, the Heyd–Scuseria–Ernzerhof hybrid method was adopted to calculate the electronic and optical properties (Heyd et al., 2005). The weak dispersion forces were described by the DFT-D3 method proposed by Grimme et al. (2010). Due to the ignorable effect of the spin–orbit coupling (SOC) on the electronic properties of the studied system, shown in **Supplementary Figure S1**, the SOC is not employed in the calculations. The vacuum thickness was set as 25 Å to prohibit the interaction adjacent layers. Besides, the convergence criterion of the force in the simulations was 0.01 eV $Å^{-1}$, while the energy was controlled in 0.01 meV.

RESULTS AND DISCUSSION

The lattice parameters of the $MoTe_2$ and PtS_2 monolayers are optimized as 3.564 and 3.529 Å, respectively, showing a low lattice mismatch of about 0.1%, which are suitable to be constructed as a heterostructure. **Supplementary Figure S2** shows the band structures of the pristine $MoTe_2$ and PtS_2 monolayers calculated using the HSE06 functional with the indirect and direct bandgaps of 1.22 and 2.60 eV, respectively, demonstrating an agreement with the previous reports (Shao et al., 2022). Then, the MP heterostructure is constructed by considering six different highly symmetrical structures, as shown in **Supplementary Figure S3**. By calculating the binding energy, the most stable stacking configuration is decided, as shown in **Figure 1A**, that the Mo atoms are located on top of the upper S atoms, while the Te atoms are set on top of the lower S atoms. The $MoTe_2/PtS_2$ heterostructure is built by vdW forces because of the weak binding energy of about −28.10 meV $Å^{-2}$ (Ren et al., 2022b), which is lower than that in graphites (about −18 meV $Å^{-2}$) (Chen et al., 2013). The projected band structure of the MP vdW heterostructure is obtained in **Figure 1B**, suggesting an indirect bandgap of about 1.26 eV. The CBM and the VBM of the MP vdW heterostructure result from the PtS_2 and $MoTe_2$ monolayers, respectively, showing a type-II band alignment, which can separate the photogenerated electrons and holes using as a photocatalyst for water splitting (Ren et al., 2021b). In detail, when the MP vdW heterostructure obtains the energy from the light, the photogenerated electrons will move to the conduction band of the $MoTe_2$ and PtS_2 monolayers, as shown in **Figure 1C**, resulting in photogenerated holes staying at the valence band. Then, the conduction band offset (CBO) can promote the photogenerated electrons from $MoTe_2$ to PtS_2 at the conduction band, while the photogenerated holes will be transferred from PtS_2 to $MoTe_2$ at the valence band. Thus, the photogenerated charges in the MP vdW heterostructure are prevented from recombination.

Next, the external biaxial strain is applied in the MP vdW heterostructure to explore its effect on the electronic structure.

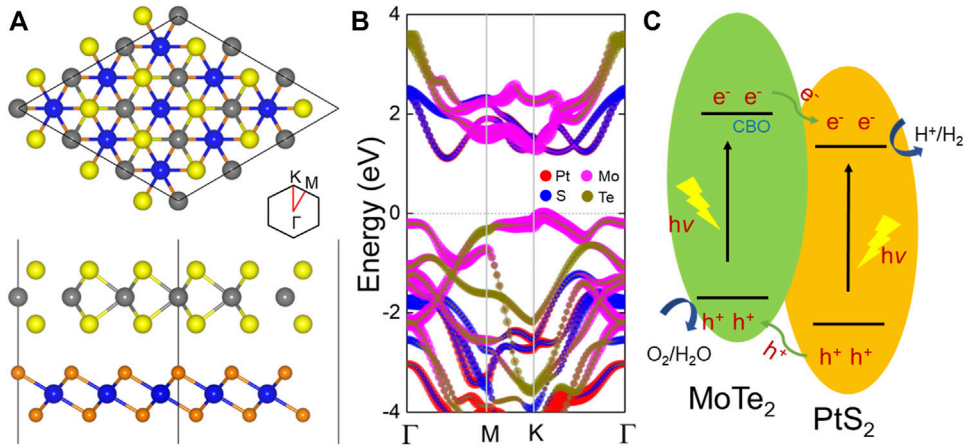

FIGURE 1 | (A) Geometric and **(B)** band structure of the MP heterostructure with the lowest binding energy. **(C)** Photogenerated charge migration path in the MP vdW heterostructure. The yellow, gray, orange, and blue spheres represent the Te, Mo, S, and Pt atoms, respectively. The Fermi level is decided as 0 shown by the gray dashed line.

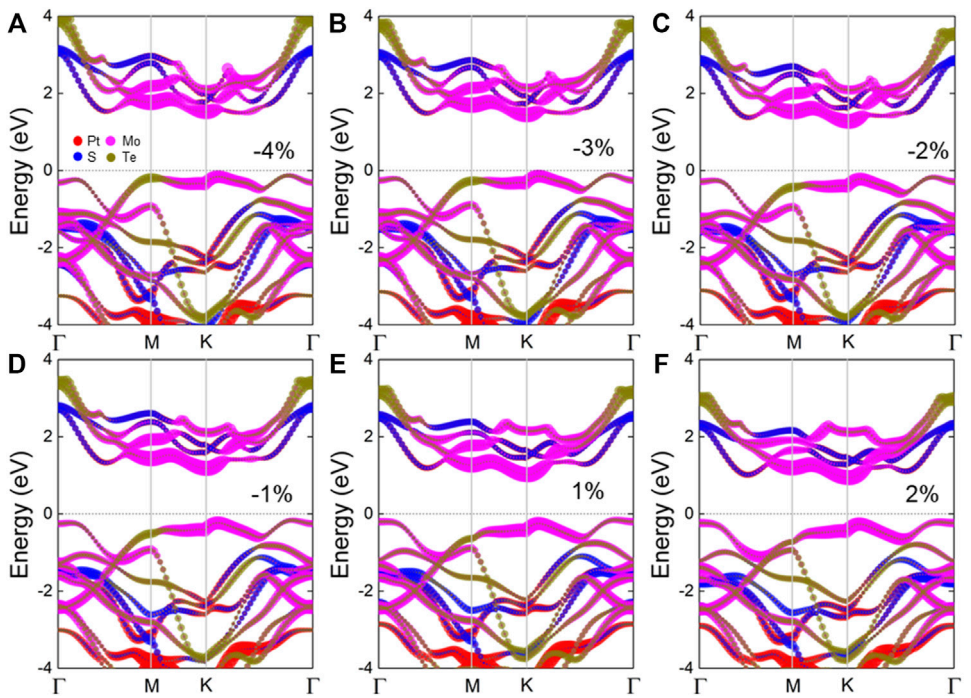

FIGURE 2 | Band structures of the MP vdW heterostructure under the external strains of **(A)** –4%, **(B)** –3%, **(C)** –2%, **(D)** –1%, **(E)** 1%, and **(F)** 2%.

In **Figure 2**, the projected band structure of the MP vdW heterostructure under the external biaxial strain from –4 to 2% is obtained, where negative and positive values represent pressure and tension, respectively. One can see that the type-II band structure is retained in the MP vdW heterostructure with that strain, which still can separate the photogenerated electrons and holes, while the bandgap decreased from 1.454 to 1.150 eV by the external biaxial strain from –4 to 2%, as shown in **Figure 3A**. In addition, the binding energy (E_b) is also investigated, which is decided by

$$E_b = E_H - E_M - E_P, \tag{1}$$

where E_H, E_M, and E_P represent the total energy of the MP vdW heterostructure, pristine $MoTe_2$, and PtS_2, respectively. The calculated binding energy change of the MP vdW heterostructure applied by different external biaxial strains is demonstrated by **Figure 3B**, which shows the stability of the MP

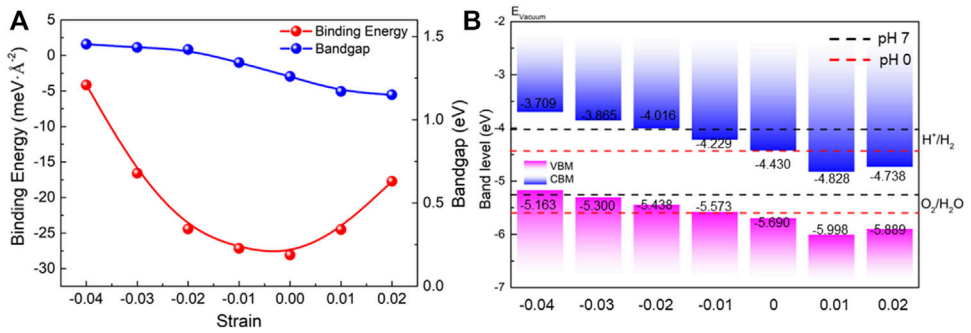

FIGURE 3 | (A) Band alignment of the MP vdW heterostructure by the external strain comparing the energy potential of the redox reaction at pH values 0 and 7. **(B)** Binding energy and the bandgap difference of the MP vdW heterostructure tuned by the external strain.

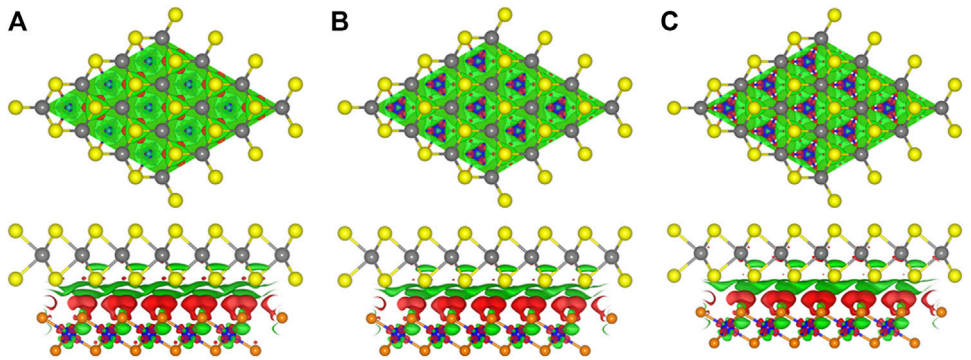

FIGURE 4 | Isosurface of the charge density difference of the MP vdW heterostructure under the strains of **(A)** –4%, **(B)** –2%, and **(C)** 2%; red and green marks demonstrate the losing and gaining of electrons, respectively. The isosurface parameter is 0.001 |e|.

vdW heterostructure, and the lowest binding energy of the MP vdW heterostructure is the unstressed state.

The band edge positions of the MP vdW heterostructure under different strains are also calculated by the HSE06 functional, demonstrated in **Figure 3B**. The potential energy values of the oxidation and reduction reactions for water splitting are −5.67 eV and −4.44 eV, respectively, at pH 0. The energy of the redox potential can be decided by the pH level with: $E = -4.44\,\text{eV} + \text{pH} \times 0.059\,\text{eV}$ for the reduction reaction, while the potential of the oxidation is obtained by $E = -5.67\,\text{eV} + \text{pH} \times 0.059\,\text{eV}$. Thus, the calculated potentials of the oxidation and reduction reactions at pH 0 are −5.26 eV and −4.03 eV, respectively, at pH 7. As a decent photocatalyst, the band edge positions of the CBM (or VBM) of the heterostructure should be higher (or lower) than the potential of the reduction (or oxidation) for water splitting (Ren et al., 2021c). In **Figure 3B**, one can see that the MP vdW heterostructure possesses suitable band edge positions to promote the redox reaction at pH 7 for water splitting by the external biaxial strains of −3% and −2%, while the MP vdW heterostructure can be used as a promising photocatalyst for water splitting at pH 0 without the external strain.

The charge density difference ($\Delta\rho$) of the MP vdW heterostructure tuned by the strain is also investigated, which is calculated as follows:

$$\Delta\rho = \rho\text{H} - \rho\text{M} - \rho\text{P}, \tag{2}$$

where ρ_H, $\rho_{M,}$ and ρ_P are used as the charge densities of the MP vdW heterostructure, pristine $MoTe_2$, and PtS_2, respectively. Under these strains, the PtS_2 layer still gains the electrons from the $MoTe_2$ layer, and the charge density difference between the interface of the MP vdW heterostructure under −4%, −2%, and 2% is demonstrated in **Figures 4A–C**, respectively. In addition, the quantitative analysis of the charge transfer in the MP vdW heterostructure is explored by the Bader charge method (Sanville et al., 2007). The calculated charge transfers between the interface of the MP vdW heterostructure under −4%, −2%, and 2% are 0.0463 |e|, 0.0475 |e|, and 0.052 |e|, respectively.

The charge density difference between the interface of the $MoTe_2$ and PtS_2 monolayers can induce a potential drop. The potential energy of the $MoTe_2$ and PtS_2 in the heterostructure by the different strains is investigated in **Figure 5**, showing that the strain can increase the potential energy of the $MoTe_2$ and PtS_2 from pressure to tension. The potential drop across the interface of the MP vdW heterostructure is obtained as 4.962, 4.720, 4.672, and 4.500 eV by the external biaxial strains of −4%, −2%, −0%, and 2%, respectively, which demonstrates the decreased charge density difference. It is worth emphasizing that such a potential

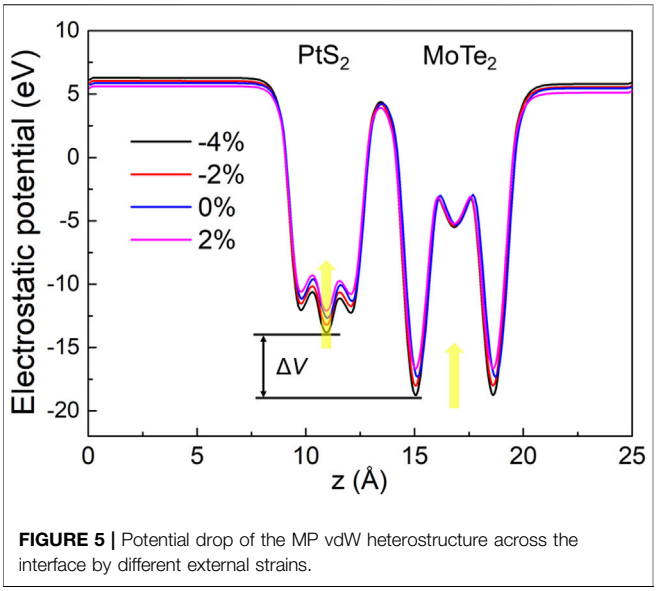

FIGURE 5 | Potential drop of the MP vdW heterostructure across the interface by different external strains.

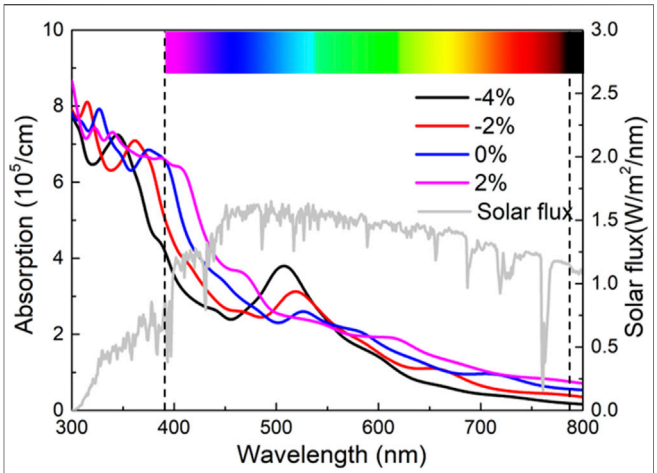

FIGURE 6 | Calculated optical absorption of the MP vdW heterostructure under the external strain.

drop in the MP vdW heterostructure can also provide a critical boost for the separation of the photogenerated electrons and holes.

We also studied the light absorption coefficient (α) of the MP vdW heterostructure by external strain using the HSE06 method, which is calculated as follows:

$$\alpha(\omega) = \frac{\sqrt{2}\omega}{c}\left\{\left[\varepsilon_1^2(\omega) + \varepsilon_2^2(\omega)\right]^{1/2} - \varepsilon_1(\omega)\right\}^{1/2}, \tag{3}$$

where ω is the angular frequency, and c is the speed of light. The real and imaginary parts are represented by $\varepsilon_1(\omega)$ and $\varepsilon_2(\omega)$, respectively. Moreover, $\varepsilon_1(\omega)$ and $\varepsilon_2(\omega)$ can be obtained as follows:

$$\varepsilon_2(q \to O_{\hat{u}}, \hbar\omega) = \frac{2e^2\pi}{\Omega\varepsilon_0}\sum_{k,v,c}\left|\langle\Psi_k^c|\hat{u}\cdot r|\Psi_k^v\rangle\right|^2 \times \delta\left(E_k^c - E_k^v - E\right), \tag{4}$$

$$\varepsilon(\omega) = \varepsilon_1(\omega) + i\varepsilon_2(\omega), \tag{5}$$

where Ψ_k, E_k, and $\hat{u}$ are the wave function, energy, and unit vector of the electric field of the incident light, respectively. The superscripts (v and c) in Ψ_k and E_k are labeled as the conduction bands and valence bands, respectively. The calculated light absorption performance of the strained MP vdW heterostructure is explained by **Figure 6** marked by a visible spectrum (Wang et al., 2018b). Evidently, applying the external compressive stress can improve the light absorption capacity at the absorption wavelength ranging from 480 to 550 nm. In detail, the light absorption peaks of the MP vdW heterostructure are obtained as $3.79 \times 10^5\,cm^{-1}$, $3.13 \times 10^5\,cm^{-1}$, and $2.60 \times 10^5\,cm^{-1}$ locating the wavelength at 509 nm, 519, and 527 nm, respectively, by the strains of −0.04, −0.02, and 0, while the light absorption performance of the MP vdW heterostructure can be enhanced by tensile stress when the absorption wavelength exceeds 550 nm. Furthermore, these obtained absorption performances are also higher than those of other 2D heterostructures, such as CdO/HfS_2 ($3.51 \times 10^5\,cm^{-1}$) (Zhang et al., 2022), arsenene/$PtSe_2$ ($2.23 \times 10^5\,cm^{-1}$) (Zheng et al., 2021), and MoSSe/GaN ($2.74 \times 10^5\,cm^{-1}$) (Ren et al., 2020c).

Furthermore, the solar-to-hydrogen efficiency of the MP vdW heterostructure is calculated by $\eta_{STH} = \eta_{abs} \times \eta_{cu}$ (Fu et al., 2018), where η_{abs} is the efficiency of light absorption, and η_{cu} demonstrates carrier utilization. As for the light absorption, it can be decided by

$$\eta_{abs} = \frac{\int_{E_g}^{\infty} P(\hbar\omega)\mathrm{d}(\hbar\omega)}{\int_0^{\infty} P(\hbar\omega)\mathrm{d}(\hbar\omega)}, \tag{6}$$

where E_g means the bandgap of the studied material. $\hbar\omega$ is used to explain the photon energy, while the AM1.5G solar energy flux is $P(\hbar\omega)$. The carrier utilization is obtained by

$$\eta_{cu} = \frac{\Delta G\int_E^{\infty}\frac{P(\hbar\omega)}{\hbar\omega}\mathrm{d}(\hbar\omega)}{\int_{E_g}^{\infty} P(\hbar\omega)\mathrm{d}(\hbar\omega)}. \tag{7}$$

To describe the potential difference in water splitting, ΔG is used by 1.23 eV here. Importantly, the photon energy of E is calculated by

$$E = \begin{cases} E_g, \left(\chi(H_2) \geq 0.2, \chi(O_2) \geq 0.6\right), \\ E_g + 0.2 - \chi(H_2), \left(\chi(H_2) < 0.2, \chi(O_2) \geq 0.6\right), \\ E_g + 0.6 - \chi(O_2), \left(\chi(H_2) \geq 0.2, \chi(O_2) < 0.6\right), \\ E_g + 0.8 - \chi(H_2) - \chi(O_2), \left(\chi(H_2) < 0.2, \chi(O_2) < 0.6\right). \end{cases} \tag{8}$$

The overpotential for the reduction and oxidation reactions for water splitting is explained by $\chi(H_2)$ and $\chi(O_2)$, respectively. In addition, previous experimental investigations provide the necessary overpotentials for the reduction and oxidation reactions as 0.2 and 0.6 eV (Fu et al., 2018), respectively. The efficiencies of light absorption of the MP vdW heterostructure

TABLE 1 | Energy conversion efficiency of light absorption, carrier utilization, and the solar-to-hydrogen efficiency of the MP vdW heterostructure under the external strain.

Strain	η_{abs} (%)	η_{cu} (%)	η_{STH} (%)
–0.03	89.44	33.66	30.10
–0.02	89.80	30.11	30.11
0	93.26	30.10	30.10

under the strains of –0.03, –0.02, and 0 are calculated by 89.44, 89.80, and 93.26%, respectively. Furthermore, the carrier utilization of the MP vdW heterostructure is 33.66, 33.53, and 32.28%, respectively, by the strains of –0.03, –0.02, and 0. Thus, the solar-to-hydrogen efficiencies are obtained as 30.10, 30.11, and 30.10%, respectively, at pH values 7, 7, and 0, as shown in **Table. 1**, which is higher than other 2D heterostructures such as CdO/arsenene (about 11.67%) (Ren et al., 2021b) and GaS/arsenene (about 25.46%) (Li et al., 2021).

CONCLUSION

In this work, the first-principles method is employed to investigate the electronic and optical performances of the MP vdW heterostructure. The external strain is also applied on the MP vdW heterostructure, and the results show that the MP vdW heterostructure maintains the type-II band alignment and decreased bandgap. In addition, the external compressive stress can tune the MP vdW heterostructure as a potential for water splitting at pH 7 because of the decent band edge positions. The strain also has a significant influence on the interfacial properties of the MP vdW heterostructure. Furthermore, the MP vdW heterostructure possesses excellent light absorption capacity and light conversion efficiency, which can also be enhanced by the strain. The results show that the MP vdW heterostructure possesses potential energy conversion used in the automotive battery system.

DATA AVAILABILITY STATEMENT

The raw data supporting the conclusions of this article will be made available by the authors, without undue reservation.

AUTHOR CONTRIBUTIONS

All the authors listed have made a substantial, direct, and intellectual contribution to the work and approved it for publication.

ACKNOWLEDGMENTS

The author LZ thanks the Zhejiang Provincial Natural Science Foundation of China (Grant No. LZY21E060002).

SUPPLEMENTARY MATERIAL

The Supplementary Material for this article can be found online at: https://www.frontiersin.org/articles/10.3389/fchem.2022.934048/full#supplementary-material

REFERENCES

Butler, S. Z., Hollen, S. M., Cao, L., Cui, Y., Gupta, J. A., Gutiérrez, H. R., et al. (2013). Progress, Challenges, and Opportunities in Two-Dimensional Materials beyond Graphene. *ACS Nano* 7, 2898–2926. doi:10.1021/nn400280c

Chang, Y.-M., Lin, C.-Y., Lin, Y.-F., and Tsukagoshi, K. (2016). Two-Dimensional MoTe$_2$ Materials: From Synthesis, Identification, and Charge Transport to Electronics Applications. *Jpn. J. Appl. Phys.* 55, 1102A1101. doi:10.7567/jjap.55.1102a1

Chen, X., Tian, F., Persson, C., Duan, W., and Chen, N.-x. (2013). Interlayer Interactions in Graphites. *Sci. Rep.* 3, 3046. doi:10.1038/srep03046

Colibaba, S. A., Körbel, S., Motta, C., El-Mellouhi, F., and Sanvito, S. (2019). Interlayer dielectric function of a type-II van der Waals semiconductor: The HfS2/PtS2 heterobilayer. *Phys. Rev. Mater.* 3, 124002. doi:10.1103/physrevmaterials.3.124002

Cui, Z., Luo, Y., Yu, J., and Xu, Y. (2021). Tuning the Electronic Properties of MoSi2N4 by Molecular Doping: A First Principles Investigation. *Phys. E Low-dimensional Syst. Nanostructures* 134, 114873. doi:10.1016/j.physe.2021.114873

Cui, Z., Wang, M., Lyu, N., Zhang, S., Ding, Y., and Bai, K. (2021). Electronic, Magnetism and Optical Properties of Transition Metals Adsorbed Puckered Arsenene. *Superlattices Microstruct.* 152, 106852. doi:10.1016/j.spmi.2021.106852

Deng, Z., and Wang, X. (2019). Strain Engineering on the Electronic States of Two-Dimensional GaN/graphene Heterostructure. *RSC Adv.* 9, 26024–26029. doi:10.1039/c9ra03175h

Fu, C.-F., Sun, J., Luo, Q., Li, X., Hu, W., and Yang, J. (2018). Intrinsic Electric Fields in Two-Dimensional Materials Boost the Solar-To-Hydrogen Efficiency for Photocatalytic Water Splitting. *Nano Lett.* 18, 6312–6317. doi:10.1021/acs.nanolett.8b02561

Geim, A. K., and Novoselov, K. S. (2007). The Rise of Graphene. *Nat. Mater* 6, 183–191. doi:10.1038/nmat1849

Grimme, S., Antony, J., Ehrlich, S., and Krieg, H. (2010). A Consistent and Accurate Ab Initio Parametrization of Density Functional Dispersion Correction (DFT-D) for the 94 Elements H-Pu. *J. Chem. Phys.* 132, 154104. doi:10.1063/1.3382344

Guo, W., Ge, X., Sun, S., Xie, Y., and Ye, X. (2020). The strain effect on the electronic properties of the MoSSe/WSSe van der Waals heterostructure: a first-principles study. *Phys. Chem. Chem. Phys.* 22, 4946–4956. doi:10.1039/d0cp00403k

Guo, Z., Miao, N., Zhou, J., Sa, B., and Sun, Z. (2017). Strain-mediated type-I/type-II transition in MXene/Blue phosphorene van der Waals heterostructures for flexible optical/electronic devices. *J. Mat. Chem. C* 5, 978–984. doi:10.1039/c6tc04349f

Heyd, J., Peralta, J. E., Scuseria, G. E., and Martin, R. L. (2005). Energy Band Gaps and Lattice Parameters Evaluated with the Heyd-Scuseria-Ernzerhof Screened Hybrid Functional. *J. Chem. Phys.* 123, 174101. doi:10.1063/1.2085170

Hong, T., Chamlagain, B., Lin, W., Chuang, H.-J., Pan, M., Zhou, Z., et al. (2014). Polarized Photocurrent Response in Black Phosphorus Field-Effect Transistors. *Nanoscale* 6, 8978–8983. doi:10.1039/c4nr02164a

Kanoun, M. B. (2018). Tuning Magnetic Properties of Two-Dimensional MoTe2 Monolayer by Doping 3d Transition Metals: Insights from First Principles Calculations. *J. Alloys Compd.* 748, 938–942. doi:10.1016/j.jallcom.2018.03.132

Kresse, G., and Furthmüller, J. (1996). Efficiency of Ab-Initio Total Energy Calculations for Metals and Semiconductors Using a Plane-Wave Basis Set. *Comput. Mater. Sci.* 6, 15–50. doi:10.1016/0927-0256(96)00008-0

Kresse, G., and Furthmüller, J. (1996). Efficient Iterative Schemes Forab Initiototal-Energy Calculations Using a Plane-Wave Basis Set. *Phys. Rev. B* 54, 11169–11186. doi:10.1103/physrevb.54.11169

Kresse, G., and Joubert, D. (1999). From Ultrasoft Pseudopotentials to the Projector Augmented-Wave Method. *Phys. Rev. B* 59, 1758–1775. doi:10.1103/physrevb.59.1758

Li, J., Huang, Z., Ke, W., Yu, J., Ren, K., and Dong, Z. (2021). High solar-to-hydrogen efficiency in Arsenene/GaX (X = S, Se) van der Waals heterostructure for photocatalytic water splitting. *J. Alloys Compd.* 866, 158774. doi:10.1016/j.jallcom.2021.158774

Li, L., Yu, Y., Ye, G. J., Ge, Q., Ou, X., Wu, H., et al. (2014). Black Phosphorus Field-Effect Transistors. *Nat. Nanotech* 9, 372–377. doi:10.1038/nnano.2014.35

Liu, G., Gan, Y., Quhe, R., and Lu, P. (2018). Strain Dependent Electronic and Optical Properties of PtS2 Monolayer. *Chem. Phys. Lett.* 709, 65–70. doi:10.1016/j.cplett.2018.08.029

Liu, Y., Cai, Y., Zhang, G., Zhang, Y.-W., and Ang, K.-W. (2017). Al-Doped Black Phosphorus P-N Homojunction Diode for High Performance Photovoltaic. *Adv. Funct. Mat.* 27, 1604638. doi:10.1002/adfm.201604638

Ma, L., Xu, Y., Zheng, J., and Dai, X. (2020). Ecodesign Method of Intelligent Boom Sprayer Based on Preferable Brownfield Process. *J. Clean. Prod.* 268, 122206. doi:10.1016/j.jclepro.2020.122206

Nguyen, C. V., Bui, H. D., Nguyen, T. D., and Pham, K. D. (2019). Controlling electronic properties of PtS2/InSe van der Waals heterostructure via external electric field and vertical strain. *Chem. Phys. Lett.* 724, 1–7. doi:10.1016/j.cplett.2019.03.048

Perdew, J. P., Burke, K., and Ernzerhof, M. (1996). Generalized Gradient Approximation Made Simple. *Phys. Rev. Lett.* 77, 3865–3868. doi:10.1103/physrevlett.77.3865

Qiu, D. Y., da Jornada, F. H., and Louie, S. G. (2013). Optical Spectrum ofMoS2: Many-Body Effects and Diversity of Exciton States. *Phys. Rev. Lett.* 111, 216805. doi:10.1103/physrevlett.111.216805

Qu, D., Liu, X., Huang, M., Lee, C., Ahmed, F., Kim, H., et al. (2017). Carrier-Type Modulation and Mobility Improvement of Thin MoTe2. *Adv. Mat.* 29, 1606433. doi:10.1002/adma.201606433

Radisavljevic, B., Radenovic, A., Brivio, J., Giacometti, V., and Kis, A. (2011). Single-layer MoS2 Transistors. *Nat. Nanotech* 6, 147–150. doi:10.1038/nnano.2010.279

Ren, K., Liu, X., Chen, S., Cheng, Y., Tang, W., and Zhang, G. (2020). Remarkable Reduction of Interfacial Thermal Resistance in Nanophononic Heterostructures. *Adv. Funct. Mat.* 30, 2004003. doi:10.1002/adfm.202004003

Ren, K., Luo, Y., Wang, S., Chou, J.-P., Yu, J., Tang, W., et al. (2019). A van der Waals Heterostructure Based on Graphene-like Gallium Nitride and Boron Selenide: A High-Efficiency Photocatalyst for Water Splitting. *ACS Omega* 4, 21689–21697. doi:10.1021/acsomega.9b02143

Ren, K., Qin, H., Liu, H., Chen, Y., Liu, X., and Zhang, G. (2022). Manipulating Interfacial Thermal Conduction of 2D Janus Heterostructure via a Thermo-Mechanical Coupling. *Adv. Funct. Mater.* 32, 2110846. doi:10.1002/adfm.202110846

Ren, K., Shu, H., Huo, W., Cui, Z., and Xu, Y. (2022c). Tuning Electronic, Magnetic and Catalytic Behaviors of Biphenylene Network by Atomic Doping. *Nanotechnology* 33, 345701.

Ren, K., Shu, H., Huo, W., Cui, Z., Yu, J., and Xu, Y. (2021). Mechanical, Electronic and Optical Properties of a Novel B2P6 Monolayer: Ultrahigh Carrier Mobility and Strong Optical Absorption. *Phys. Chem. Chem. Phys.* 23, 24915–24921. doi:10.1039/d1cp03838a

Ren, K., Sun, M., Luo, Y., Wang, S., Yu, J., and Tang, W. (2019). First-principle Study of Electronic and Optical Properties of Two-Dimensional Materials-Based Heterostructures Based on Transition Metal Dichalcogenides and Boron Phosphide. *Appl. Surf. Sci.* 476, 70–75. doi:10.1016/j.apsusc.2019.01.005

Ren, K., Tang, W., Sun, M., Cai, Y., Cheng, Y., and Zhang, G. (2020). A direct Z-scheme PtS2/arsenene van der Waals heterostructure with high photocatalytic water splitting efficiency. *Nanoscale* 12, 17281–17289. doi:10.1039/d0nr02286a

Ren, K., Wang, S., Luo, Y., Chou, J.-P., Yu, J., Tang, W., et al. (2020). High-efficiency photocatalyst for water splitting: a Janus MoSSe/XN (X = Ga, Al) van der Waals heterostructure. *J. Phys. D. Appl. Phys.* 53, 185504. doi:10.1088/1361-6463/ab71ad

Ren, K., Zheng, R., Xu, P., Cheng, D., Huo, W., Yu, J., et al. (2021). Electronic and Optical Properties of Atomic-Scale Heterostructure Based on MXene and MN (M = Al, Ga): A DFT Investigation. *Nanomaterials* 11, 2236. doi:10.3390/nano11092236

Ren, K., Zheng, R., Yu, J., Sun, Q., and Li, J. (2021). Band Bending Mechanism in CdO/Arsenene Heterostructure: A Potential Direct Z-Scheme Photocatalyst. *Front. Chem.* 9, 788813. doi:10.3389/fchem.2021.788813

Ren, K., Zhu, Z., Wang, K., Huo, W., and Cui, Z. (2022). Stacking-Mediated Type-I/Type-II Transition in Two-Dimensional MoTe2/PtS2 Heterostructure: A First-Principles Simulation. *Crystals* 12, 425. doi:10.3390/cryst12030425

Sajjad, M., Singh, N., and Schwingenschlögl, U. (2018). Strongly Bound Excitons in Monolayer PtS2 and PtSe2. *Appl. Phys. Lett.* 112, 043101. doi:10.1063/1.5010881

Sanville, E., Kenny, S. D., Smith, R., and Henkelman, G. (2007). Improved Grid-Based Algorithm for Bader Charge Allocation. *J. Comput. Chem.* 28, 899–908. doi:10.1002/jcc.20575

Shao, C., Ren, K., Huang, Z., Yang, J., and Cui, Z. (2022). Two-Dimensional PtS2/MoTe2 van der Waals Heterostructure: An Efficient Potential Photocatalyst for Water Splitting. *Front. Chem.* 10, 847319. doi:10.3389/fchem.2022.847319

Shen, Z., Ren, K., Zheng, R., Huang, Z., Cui, Z., Zheng, Z., et al. (2022). The Thermal and Electronic Properties of the Lateral Janus MoSSe/WSSe Heterostructure. *Front. Mat.* 9, 838648. doi:10.3389/fmats.2022.838648

Shi, D., Wang, G., Li, C., Shen, X., and Nie, Q. (2017). Preparation and Thermoelectric Properties of MoTe 2 Thin Films by Magnetron Co-sputtering. *Vacuum* 138, 101–104. doi:10.1016/j.vacuum.2017.01.030

Sun, M., Chou, J.-P., Ren, Q., Zhao, Y., Yu, J., and Tang, W. (2017). Tunable Schottky barrier in van der Waals heterostructures of graphene and g-GaN. *Appl. Phys. Lett.* 110, 173105. doi:10.1063/1.4982690

Sun, M., Chou, J.-P., Yu, J., and Tang, W. (2017). Effects of Structural Imperfection on the Electronic Properties of graphene/WSe2 Heterostructures. *J. Mat. Chem. C* 5, 10383–10390. doi:10.1039/c7tc03131a

Sun, M., Luo, Y., Yan, Y., and Schwingenschlögl, U. (2021). Ultrahigh Carrier Mobility in the Two-Dimensional Semiconductors B8Si4, B8Ge4, and B8Sn4. *Chem. Mat.* 33, 6475–6483. doi:10.1021/acs.chemmater.1c01824

Sun, M., and Schwingenschlögl, U. (2020). δ-CS: A Direct-Band-Gap Semiconductor Combining Auxeticity, Ferroelasticity, and Potential for High-Efficiency Solar Cells. *Phys. Rev. Appl.* 14, 044015. doi:10.1103/physrevapplied.14.044015

Sun, M., and Schwingenschlögl, U. (2021). Structure Prototype Outperforming MXenes in Stability and Performance in Metal-Ion Batteries: A High Throughput Study. *Adv. Energy Mat.* 11, 2003633. doi:10.1002/aenm.202003633

Sun, M., Yan, Y., and Schwingenschlögl, U. (2020). Beryllene: A Promising Anode Material for Na- and K-Ion Batteries with Ultrafast Charge/Discharge and High Specific Capacity. *J. Phys. Chem. Lett.* 11, 9051–9056. doi:10.1021/acs.jpclett.0c02426

Wang, G.-Z., Chang, J.-L., Tang, W., Xie, W., and Ang, Y. S. (2022b). 2D Materials and Heterostructures for Photocatalytic Water-Splitting: A Theoretical Perspective. *J. Phys. Phys. D. Appl. Phys.* 55, 293002.

Wang, G., Chang, J., Tang, W., Xie, W., and Ang, Y. S. (2022a). 2D Materials and Heterostructures for Photocatalytic Water-Splitting: a Theoretical Perspective. *J. Phys. D. Appl. Phys.* 55, 293002. doi:10.1088/1361-6463/ac5771

Wang, G., Gong, L., Li, Z., Wang, B., Zhang, W., Yuan, B., et al. (2020). A Two-Dimensional CdO/CdS Heterostructure Used for Visible Light Photocatalysis. *Phys. Chem. Chem. Phys.* 22, 9587–9592. doi:10.1039/d0cp00876a

Wang, G., Zhang, L., Li, Y., Zhao, W., Kuang, A., Li, Y., et al. (2020). Biaxial Strain Tunable Photocatalytic Properties of 2D ZnO/GeC Heterostructure. *J. Phys. D. Appl. Phys.* 53, 015104. doi:10.1088/1361-6463/ab440e

Wang, G., Zhi, Y., Bo, M., Xiao, S., Li, Y., Zhao, W., et al. (2020). 2D Hexagonal Boron Nitride/Cadmium Sulfide Heterostructure as a Promising Water-Splitting Photocatalyst. *Phys. Status Solidi B* 257, 1900431. doi:10.1002/pssb.201900431

Wang, S., Ren, C., Tian, H., Yu, J., and Sun, M. (2018). MoS2/ZnO van der Waals heterostructure as a high-efficiency water splitting photocatalyst: a first-principles study. *Phys. Chem. Chem. Phys.* 20, 13394–13399. doi:10.1039/c8cp00808f

Wang, S., Tian, H., Ren, C., Yu, J., and Sun, M. (2018). Electronic and Optical Properties of Heterostructures Based on Transition Metal Dichalcogenides and Graphene-like Zinc Oxide. *Sci. Rep.* 8, 12009. doi:10.1038/s41598-018-30614-3

Wang, S., Ukhtary, M. S., and Saito, R. (2020). Strain Effect on Circularly Polarized Electroluminescence in Transition Metal Dichalcogenides. *Phys. Rev. Res.* 2, 033340. doi:10.1103/physrevresearch.2.033340

Wickramaratne, D., Zahid, F., and Lake, R. K. (2014). Electronic and Thermoelectric Properties of Few-Layer Transition Metal Dichalcogenides. *J. Chem. Phys.* 140, 124710. doi:10.1063/1.4869142

You, B., Wang, X., Zheng, Z., and Mi, W. (2016). Black phosphorene/monolayer transition-metal dichalcogenides as two dimensional van der Waals heterostructures: a first-principles study. *Phys. Chem. Chem. Phys.* 18, 7381–7388. doi:10.1039/c5cp07585h

Zhang, H., Chhowalla, M., and Liu, Z. (2018). 2D Nanomaterials: Graphene and Transition Metal Dichalcogenides. *Chem. Soc. Rev.* 47, 3015–3017. doi:10.1039/c8cs90048e

Zhang, Q., Ren, K., Zheng, R., Huang, Z., An, Z., and Cui, Z. (2022). First-Principles Calculations of Two-Dimensional CdO/HfS2 Van der Waals Heterostructure: Direct Z-Scheme Photocatalytic Water Splitting. *Front. Chem.* 10, 879402. doi:10.3389/fchem.2022.879402

Zhao, D., Xie, S., Wang, Y., Zhu, H., Chen, L., Sun, Q., et al. (2019). Synthesis of Large-Scale Few-Layer PtS2 Films by Chemical Vapor Deposition. *AIP Adv.* 9, 025225. doi:10.1063/1.5086447

Zheng, R., Ren, K., Yu, J., Zhu, Z., and Sun, Q. (2021). Type-II Heterostructure Based on two-Dimensional Arsenene and PtS_2 With Novel Light Absorption Performance. Third International Conference on Optoelectronic Science and Materials (ICOSM 2021), Hefei, China, December 9, 2021 (SPIE), 182–186.

Conflict of Interest: The authors declare that the research was conducted in the absence of any commercial or financial relationships that could be construed as a potential conflict of interest.

Publisher's Note: All claims expressed in this article are solely those of the authors and do not necessarily represent those of their affiliated organizations, or those of the publisher, the editors, and the reviewers. Any product that may be evaluated in this article, or claim that may be made by its manufacturer, is not guaranteed or endorsed by the publisher.